Tip-enhanced dark exciton nano-imaging and local strain control in WSe_2 : Supporting Information

Kathryn Hasz,[1,2] Zuocheng Hu,[1] Kyoung Duck Park,[3] and Markus B. Raschke[1,*]

[1]*Department of Physics, and JILA, University of Colorado, Boulder, CO 80309, USA*

[2]*Department of Physics, Carthage College, Kenosha, WI 53140*

[3]*Department of Physics, Pohang University of Science and Technology (POSTECH), 77, Cheongam-ro, Pohang, 37673, Republic of Korea*

(Dated: December 5, 2022)

FORCE-DISTANCE CURVES

Performing tip-enhanced spectroscopy under well defined tip-sample force values is particularly challenging in conventional shear-force AFM typically used for TEPL and tip-enhanced Raman scattering (TERS) [1]. In contrast, with cantilever tips of known force constant and the ability for quantitative deflection measurement, tip-sample forces can be derived and correlated with the near-field signal [2, 3].

Fig. S1 shows a typical force-distance approach curve. The point of snap-in due to the compliance of the cantilever is indicated with the red arrow. The nominally negative distance values indicate that the tip in the repulsive regime gives rise to the cantilever now being deflected upward by the tip-sample force. Conversely, that deflection leads to an increasing force onto the sample, which we correlate with the change in exciton intensity as discussed in the main text. The behavior is repeatable and reversible, suggesting that there is little to no change in tip geometry during the measurement process within the range of force applied. Data for the 2D scans shown for Figs. 2 and 3 in the main manuscript were taken at a applied force of +5 nN.

The linearity of the portion of the force-distance curve in contact and the repeatability for the measurement whether approaching the surface or retracting from it suggests that the materials remain in the elastic regime. It is still a weakly perturbative regime, whereas as at high strain, the bandstructure of the monolayer can can change from a direct to an indirect bandgap as the preferential K-K point transition gives way to a K-Γ transition [4, 5]. However, these strain and Purcell effects are the intertwining sources of the preferential excitement of dark excitons on areas of more extreme topography.

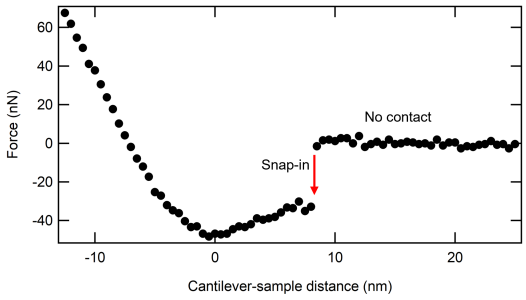

Fig. S1. Force-distance curve while approaching the sample. The point of snap-in is indicated by the red arrow. Negative force values correspond to deflection of cantilever in the repulsive regime, providing calibrated application of force to induce controlled sample strain.

DARK VS. BRIGHT EXCITON RELATIVE ENHANCEMENT

The ratio between the TEPL intensity of the dark exciton to the bright exciton emission is shown in Fig. S2. It shows enhancement of dark exciton emission in selected areas, most notably the area indicated by the yellow circle. That area corresponds to the same area indicated by the yellow circle in Fig. 2 of the main text in which we see a strong dark exciton but weak bright exciton. The increase of relative dark exciton intensity beyond that of the bright exciton indicates a decoupling of dark vs. bright exciton emission.

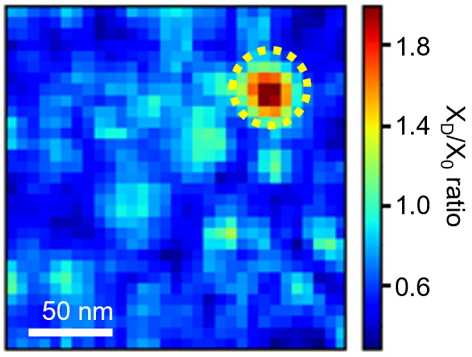

Fig. S2. Intensity ratio between dark and bright exciton TEPL emission, indicating areas of decoupling with exceptionally high dark exciton emission contrast.

STRAIN LOCALIZED EXCITONS

In certain spatial locations, strain localized excitons are seen. These occurr in areas with bubbles as we applied a localized force on the bubble with the AFM tip. An example is given in Fig. S3. The behavior is reversible and repeatable at the same location. The dark exciton is distinct from the strain localized exciton. It has an onset at lower strain and emits at a higher energy. While localized excitons warrant further investigation in their own right, the study of strain localized excitons is outside the scope of this work.

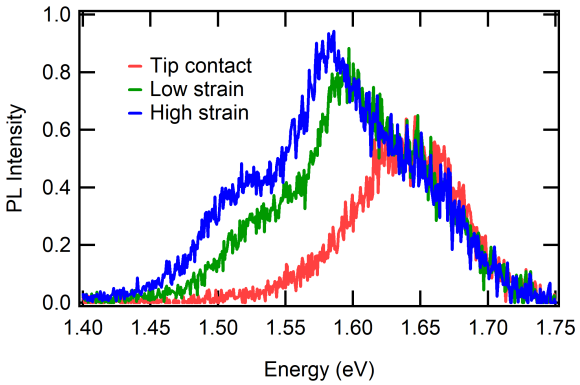

Fig. S3. A strain localized exciton with its characteristic low energy emission is apparent in some TEPL measurements. It emerges at energies of ~ 1.52 eV, i.e., ca. 80 meV below the dark exciton emission. The emergence of the strain localized exciton gives rise to an apparent shift of the dark exciton peak due to the spectral overlap.

PEAK POSITIONS OF DARK AND BRIGHT EXCITON EMISSION

The spatial distribution of TEPL peak positions of bright (a) and dark exciton (b) emission is shown in Fig. S4 (same data as Fig. 3 in main text). A next nearest neighbor pixel averaging is applied for better visualization of the key spatial features due to limited signal-to-noise in this type of analysis. Here we analyze the areas marked by blue and red dashed lines which indicate the same areas as in Fig. 2 of the main text. Similar to the intensity data in Fig. 2c and d, the area in the yellow circle shows a much greater change, here for the dark exciton spectral position than that for the bright exciton.

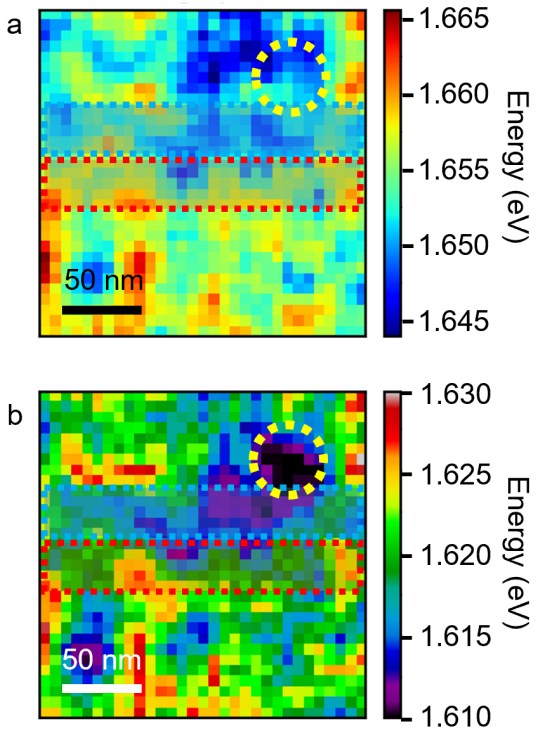

Fig. S4. Image of spectral peak positions for bright exciton (a) and dark exciton (b) TEPL emission.

Two example cross sections of peak positions and corresponding strain are shown in Fig. S5, corresponding to the blue (a,b, and c) and red (d,e, and f) areas of Fig. S4. Similar to the data in Fig. 3, a correlated spectral shift of bright and dark exciton peak positions is observed, both red-shifting with increasing tensile strain. This behavior is consistent with past work investigating the energy shift due to global strain [6] and tip-induced local strain control.[1]

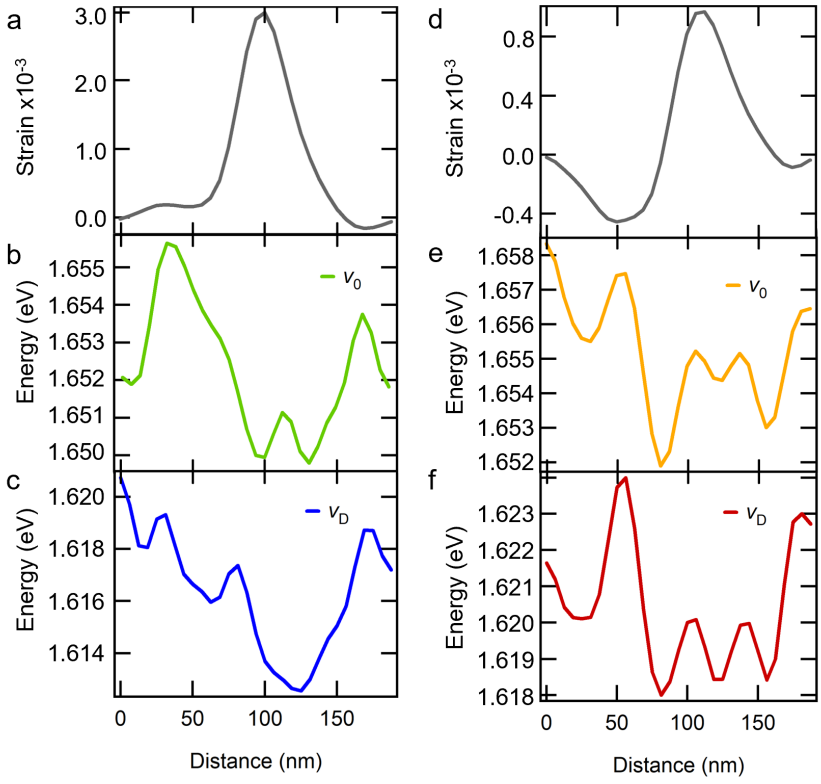

Fig. S5. Averaged cross sections of peak positions from Fig. S4a,b and strain from Fig. 2b in the main text. Show are strain, bright exciton position, and dark exciton position, respectively, for the blue (a,b, and c) and red band (d,e, and f) with correlated red-shift of both excitons with decreasing compressive and increasing tensile strain.

Fig. S6 shows an analysis of the correlation of strain with TEPL peak position for all data from the blue and red areas indicated in Fig. S4. The wide range of scatter we attribute to the superposition of different clusters of data, and effects other than curvature induced strain. Different sample regions with different local strain from exfoliation, defects, and other structural heterogeneities give rise to different initial PL peak energies, which in turn may respond differently to externally induced strain.

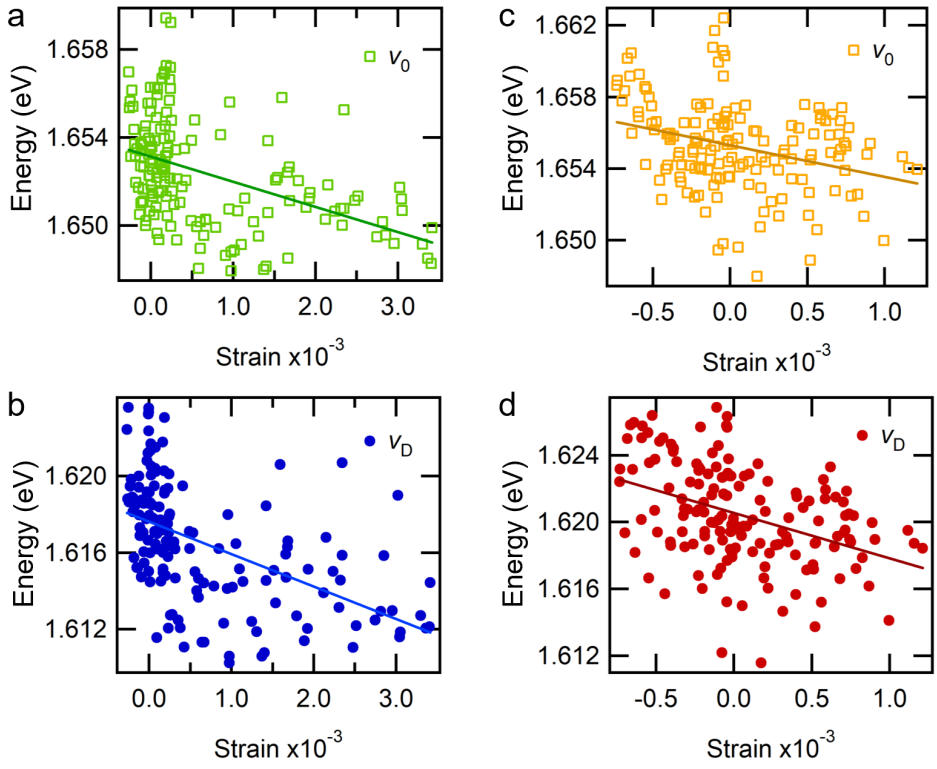

Fig. S6. Position vs. strain of the data from Fig. S5b-c,e-f. The larger scatter compared to that seen in Fig. 3 (main text) is due to the superposition of different clusters with different initial strain or peak positions due to variations in substrate interaction, defects, etc. affecting initial peak position and sensitivity with respect to strain.

ADDITIONAL DATA

Another dataset showing the strain-localized behavior on a separate 100x100 nm^2 area of the sample is presented in Fig. S7. Fig.S7a shows the AFM topography, and Fig. S7b shows the corresponding strain map calculated following Darlington *et al.* [7]. Equivalent to the data presented

in the main text, we perform full spatio-spectral imaging and analyze the bright and dark exciton emission with spectral fitting to each image pixel. Fig. S7c and d show the bright and dark exciton intensity maps, respectively. Fig. S7e and f show the bright and dark exciton position maps, respectively. Image data are smoothed with a three point filter to reduce scatter from fitting errors.

Similar to the data presented in the main text, we see a correlation between the sample topography (a), strain (b), and bright (c) and dark (d) exciton intensities. A higher strain corresponds to a higher PL intensity. While the correlation of strain with exciton peak position is again less exact, there are areas where the peak position is redshifted along with a higher tensile strain.

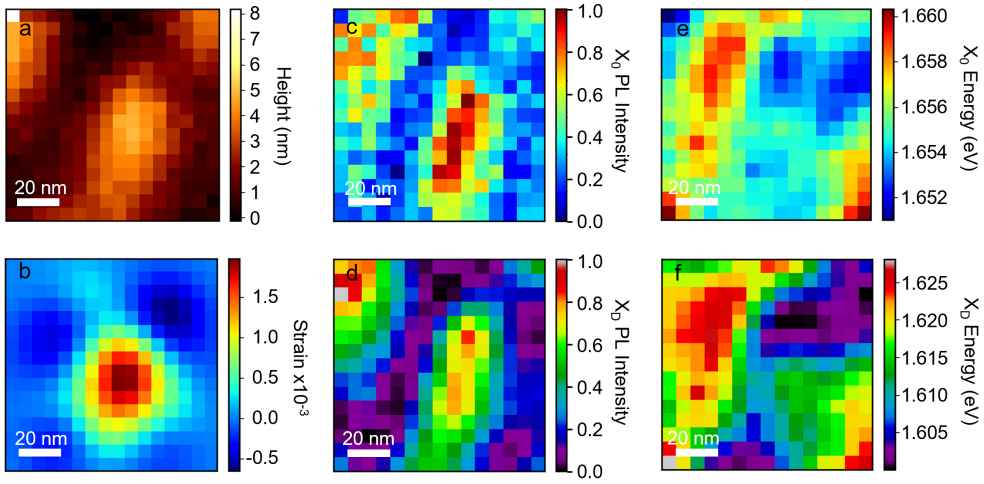

Fig. S7. Topography (a), strain (b), bright exciton intensity (c), dark exciton intensity (d), bright exciton position (e), and dark exciton position (f) across a separate 100 x 100 nm^2 scan area of monolayer WSe_2 .

DATA AVAILABILITY

The data generated in this study are available upon request.

* markus.raschke@colorado.edu

[1] Park, K. D. *et al.* Hybrid tip-enhanced nanospectroscopy and nanoimaging of monolayer WSe_2 with local strain control. *Nano Letters* **16**, 2621–2627 (2016).

[2] Watanabe, H., Ishida, Y., Hayazawa, N., Inouye, Y. & Kawata, S. Tip-enhanced near-field raman analysis of tip-pressurized adenine molecule. *Physical Review B* **69**, 155418 (2004).

[3] Yano, T.-a., Verma, P., Saito, Y., Ichimura, T. & Kawata, S. Pressure-assisted tip-enhanced Raman imaging at a resolution of a few nanometres. *Nature Photonics* **3**, 473–477 (2009).

[4] Blundo, E. *et al.* Evidence of the direct-to-indirect band gap transition in strained two-dimensional WS_2, MoS_2, and WSe_2. *Physical Review Research* **2**, 1–7 (2020).

[5] Cianci, S., Blundo, E., Felici, M., Polimeni, A. & Pettinari, G. Tailoring the optical properties of 2D transition metal dichalcogenides by strain. *Optical Materials* **125**, 112087 (2022).

[6] Castellanos-Gomez, A. *et al.* Local strain engineering in atomically thin MoS_2. *Nano letters* **13**, 5361–5366 (2013).

[7] Darlington, T. P. *et al.* Facile and quantitative estimation of strain in nanobubbles with arbitrary symmetry in 2D semiconductors verified using hyperspectral nano-optical imaging. *Journal of Chemical Physics* **153**, 024702 (2020).